Mechanical loading induces distinct and shared responses in endothelial and muscle cells and reveals exercise-like molecular profiles

Sakari Mäntyselkä[1*], Erik Niemi[1*], Laura Ylä-Outinen[1], Kalle Kolari[1], Liina Uusitalo-Kylmälä[1], Alfredo Ortega-Alonso[1], Roosa-Maria Liimatainen[2], Vasco Fachada[1], Perttu Permi[2,3,4], Elina Kalenius[2], Juha J Hulmi[1#], Riikka Kivelä[1,5,6#]

[1]Faculty of Sport and Health Sciences, NeuroMuscular Research Center, University of Jyväskylä, Jyväskylä, Finland
[2]Department of Chemistry, University of Jyväskylä, Jyväskylä, Finland
[3]Department of Biological and Environmental Science, University of Jyväskylä, Jyväskylä, Finland
[4]Institute of Biotechnology, Helsinki Institute of Life Science, University of Helsinki, Helsinki, Finland
[5]Stem Cells and Metabolism Research Program, Research Programs Unit, Faculty of Medicine, University of Helsinki, Helsinki, Finland
[6]Wihuri Research Institute, Helsinki, Finland

* Equal contribution as first authors

# Equal contribution as senior authors

Correspondence to Riikka Kivelä (riikka.m.kivela@jyu.fi) & Juha J Hulmi (juha.hulmi@jyu.fi), NeuroMuscular Research Center, Faculty of Sport and Health Sciences, University of Jyväskylä, Rautpohjankatu 8, 40014 Finland

Keywords

Acetate, Development, Metabolomics, PHGDH, Serine, Transcriptomics

Abstract

Skeletal muscles and blood vessels are continuously exposed to mechanical forces, particularly during exercise. We subjected human endothelial and skeletal muscle cells to cyclic mechanical stretch and investigated acute molecular responses. Mechanical loading elicited both shared and cell type-specific alterations in transcriptomic and metabolomic profiles, several of which mirror changes observed in vivo following exercise. Notably, both cell types released acetate in response to mechanical loading, however, many of the changes occurred in opposite directions. For example, genes associated with the electron transport chain were repressed in endothelial cells but upregulated in skeletal muscle cells. Furthermore, mechanical loading promoted a transcriptomic shift in endothelial cells indicative of maturation, and reduced their proliferation. Metabolic changes were more pronounced in endothelial cells, which exhibited increased serine biosynthesis from glucose, as demonstrated by ^{13}C-(U)-glucose tracing. Further experiments targeting phosphoglycerate dehydrogenase (PHGDH), a key enzyme in the serine synthesis pathway, underscored its role in endothelial cell anabolism. These findings suggest that mechanical loading alone can recapitulate several exercise-induced effects in endothelial and muscle cells, and highlight a potential link between mechanical stimuli, serine synthesis, and endothelial cell maturation.

Introduction

Skeletal muscle is a highly vascularized tissue and myofibers and endothelial cells together make up ~70% of the total nuclei count in skeletal muscle tissue (1, 2). Myofibers are contractile cells that both produce and sense mechanical forces. Endothelial cells lining the blood vessels sense mechanical forces produced by blood flow (shear stress) and by contracting and stretching muscle. In skeletal muscle, mechanical forces are produced and sensed especially during exercise, which can be mimicked *in vitro* using contraction and stretching models (3, 4). Previously, it has been demonstrated that cyclic mechanical loading (i.e. cyclic stretching) induces a wide variety of molecular and morphological responses in endothelial [reviewed in (5)] and muscle cells [reviewed in (6)]. For example, mechanical loading has been found to activate the mechanistic target of rapamycin complex 1 (mTORC1) (7) and to induce highly similar gene expression changes in murine myofiber-like multinucleated cells (myotubes) as resistance exercise *in vivo* in myofibers (8). Still, studies using human muscle cells are needed (4). Endothelial cells, in turn, have been shown to migrate and change orientation in response to stretch, secrete angiocrines, and activate angiogenesis-related pathways (5, 9, 10), which also occur in response to exercise and increased blood flow *in vivo* (11, 12). However, there are only a few studies (9, 13, 14) investigating the remodeling of the global molecular landscape in response to mechanical loading, and none in comparing the responses in different cell types. It is recently acknowledged that endothelial and muscle cell cross-talk is essential in regulating the development, maintenance, and repair of muscle tissue [reviewed in (2)].

Skeletal muscle responses to mechanical loading *in vivo* have mostly been examined using mixed muscle samples, which lack cell-specificity as skeletal muscle contains over 10 different cell types (1). *In vitro* models allow us to study metabolic responses in a cell type-specific manner. However, according to our knowledge, there are no studies in which the mechanical loading-induced responses of muscle and endothelial cells have been compared. Exercise induces many metabolic changes, such as increased glycolysis and oxidative phosphorylation at the whole-muscle level (15). However, little is known about how exercise or mechanical loading *per se* affects other metabolic pathways, such as those branching from glycolysis (e.g., the pentose phosphate and serine synthesis pathways), and their role in exercise responses such as angiogenesis. Previously, mechanical stretching of liver endothelial cells during vasodilation was demonstrated to induce angiocrine signals that support liver growth and survival, and potentially contribute to liver regeneration (10). Blood vessels in skeletal muscles experience immediate vasodilation—and thus endothelial cell stretching—when their physiological function is rapidly changed during exercise.

Here we explored how mechanical loading affects the transcriptional landscape and metabolomics of two different human endothelial cell lines, and primary human skeletal muscle cells, to mimic exercise on-a-dish and to study cell type-specific responses. Molecular responses resembled changes typically observed after exercise *in vivo*, however, many pathways were changed in opposite directions in endothelial cells and

muscle cells, demonstrating highly cell type-specific responses. The current exercise-on-a-dish model induced acetate secretion from both cell types, suggesting its potential role as an exerkine.

Results

Mechanical loading induced cell type-specific transcriptomic changes mirroring exercise-induced responses

We first investigated the transcriptomic changes in two human endothelial cell lines (HUVEC & HCMEC) as well as human skeletal muscle cells (HSkM) (Fig. 1A). The used mechanical loading scheme did not induce detachment of the cells, significant membrane damage, or cell death in either muscle or endothelial cells as determined by total RNA yield and the extracellular lactate dehydrogenase (LDH) activity assay (Supplementary Fig. 1A-B). Differential gene expression analysis demonstrated that all three cell types presented significant changes in their transcriptomes in response to the mechanical loading, as demonstrated by the principal component analysis (PCA) (Fig. 1B). The transcriptomic response was the largest in HUVECs, with the total number of differentially expressed genes being approximately 3-fold larger than in HCMECs or HSkM cells (Fig. 1C). In HUVECs, 717 genes were significantly upregulated, and 779 genes significantly downregulated ($\log_2 FC \geq 0.5$ & adj. $p \leq 0.05$), for HCMECs, 241 genes were upregulated, and 261 genes were downregulated, and in HSkM cells 262 genes were upregulated and 126 genes were downregulated. The ten most upregulated and downregulated genes by indexing in order of magnitude and consistency of change (Log_2FC and adj. p) are annotated in Figure 1D for each cell type. For the complete lists of differentially expressed genes and their full names, please refer to Supplementary Table S1.

When comparing overlaps in both up- and downregulated genes in all three cell lines, we noticed that the two endothelial cell lines clearly demonstrated similarities in their gene expression, whereas the overlaps between endothelial cells and muscle cells were small (Fig. 1E). Only one gene was upregulated (*CREB5*) and one gene was downregulated (*FAM43A*) in all three cell lines in response to mechanical loading. For the complete lists of overlapping differentially expressed genes, please refer to Supplementary Table S2. These results demonstrated greater transcriptomic responses to mechanical loading in endothelial cells than in muscle cells. Large overlaps in gene expression could be seen between the endothelial cell lines, whereas endothelial cells and muscle cells responded differently, highlighting the cell type-specificity.

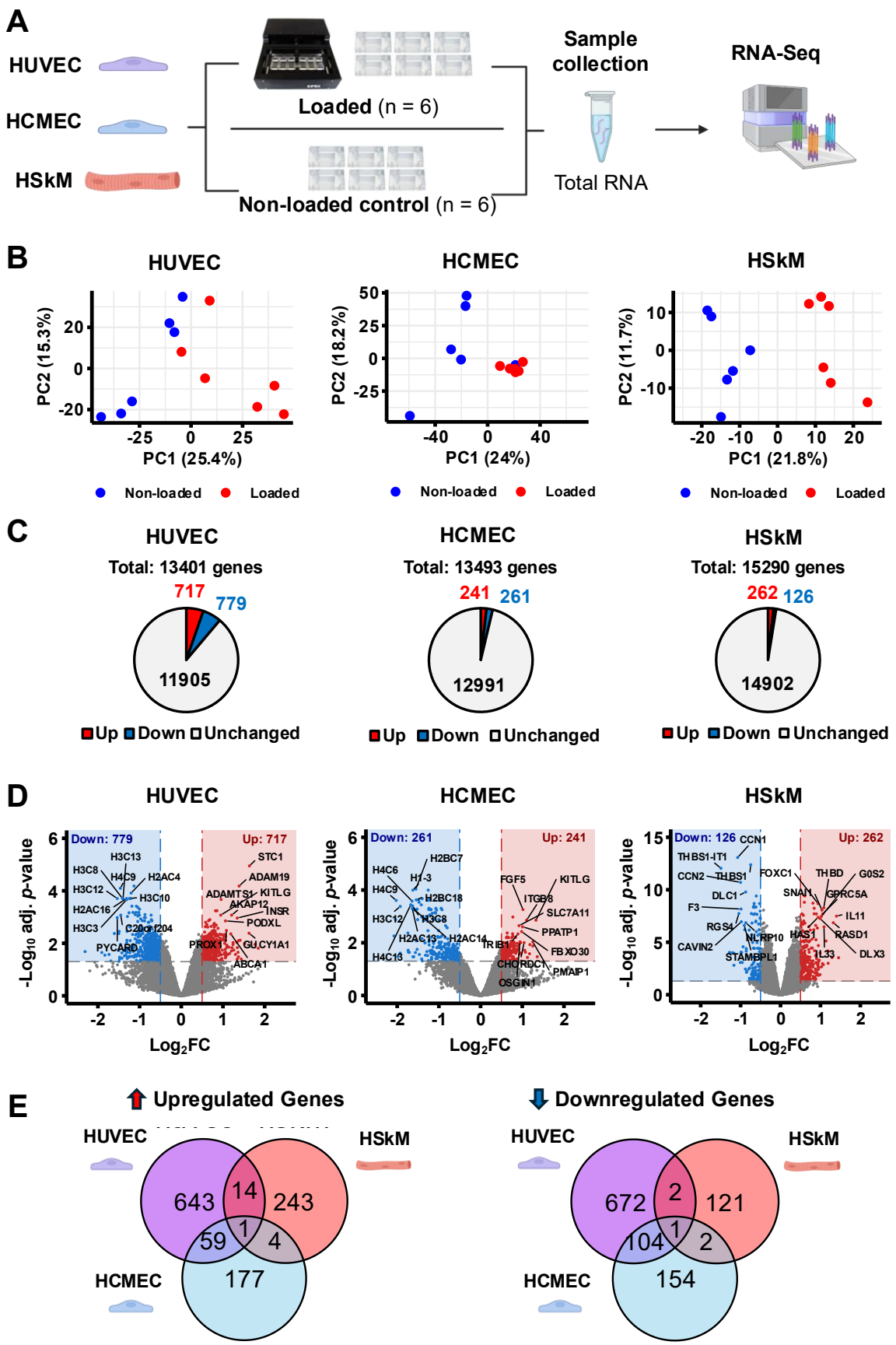

Fig. 1 Changes in gene expression of human endothelial cells (HUVECs, HCMECs) and muscle cells (HSkM) in response to mechanical loading. **A)** Schematic representation of experimental

design. The experiment was repeated for each cell line separately. Cells from one stretching chamber were used as one sample for RNA-Seq. **B)** PCA plots of samples in each cell line respectively. **C)** The total number of detected genes and the number of genes that were either up- or downregulated ($\log_2$FC ≥ 0.5 and adj. $p \leq 0.05$) for each cell line. **D)** Volcano plots illustrating the amounts of differentially expressed and unchanged genes in all three cell lines. Top 10 up- and downregulated genes by magnitude and consistency are annotated **E)** Venn diagrams showing the number of shared up- and downregulated genes in all three cell lines

Gene Set Enrichment Analysis (GSEA) results revealed that the two endothelial cell lines showed highly similar pathway enrichment after mechanical loading (Supplementary Table S3). Twenty Gene Ontology: Biological Processes (GO:BP) and four Reactome pathways were similarly upregulated in HUVEC and HCMEC, and 27 GO:BP, 83 Reactome and three KEGG pathways were similarly downregulated. The GSEA results of HUVECs showed upregulation of cell maturation and EC junction-related pathways such as *Endothelial cell development, Establishment of endothelial barrier, Cellular response to nitrogen compound* and *Cell junction organization* (Fig. 2A). Furthermore, out of the GO:BP *Endothelial cell development* -pathway, 18/72 genes were significantly upregulated in HUVECs in response to mechanical loading (Fig. 2B). For muscle cells, upregulated pathways were mostly related to oxidative phosphorylation (OXPHOS) and ribosome biogenesis (Fig. 2D). Many of the GSEA findings were also reproduced by the gene set overrepresentation analysis (ORA) (Supplementary Fig. 2).

To evaluate the external validity of our exercise-on-a-dish model, we analyzed the expression of common exercise-induced and mechanosensitive genes. In endothelial cells, we examined the expression of *KLF2/4*, *THDB*, *NRP2*, *YAP1*, *HIF1A*, and *NFE2L2* and VEGF receptor 1 & 2 encoding genes *FLT1* and *KDR* (Fig. 2C), which have been shown to be induced in ECs in response to flow-induced shear stress (16–18). Indeed, we found that from these genes all but *HIF1A* were significantly upregulated in HUVECs in response to the uniaxial mechanical loading. In HSkM cells, we specifically focused on exercise-altered genes myostatin (*MSTN*), *NR4A3, VEGFA, MYC, ATF3,* and *TNFRSF12A* (Fig. 2E), and observed similar changes in these genes after mechanical loading as have been shown especially in response to resistance exercise in vivo (19–22). We additionally looked at the expression of OXPHOS-related genes *PPARGC1A* and its upstream regulator *PPARD* (23–25), and found *PPARD* to be upregulated after mechanical loading, while there was no change in *PPARGC1A* expression (Fig. 2E). Together, these findings suggest that our *in vitro* mechanical loading model mimics exercise and flow-induced mechanical stress in both endothelial and muscle cells.

When comparing gene set enrichment of the endothelial cell lines to muscle cells, we found multiple pathways enriched in opposite directions in response to mechanical loading (Supplementary Table S4). In HUVECs and HSkM cells 12 GO:BP, three Reactome and two KEGG pathways were oppositely enriched and the same was true for HCMECs and HSkM cells in 14 GO:BP, four Reactome and three KEGG pathways. Five of these pathways were found to be oppositely regulated when comparing both endothelial cell types to muscle cells. These pathways were related to cellular respiration,

metabolism, and chromatin remodeling (Fig. 2F). Most prominently, OXPHOS-related pathways were downregulated in endothelial cell lines, while upregulated in muscle cells. Closer inspection revealed that gene expression was specifically affected in the same fashion throughout the electron transport chain (ETC)-complexes I-V (Fig. 2G).

171

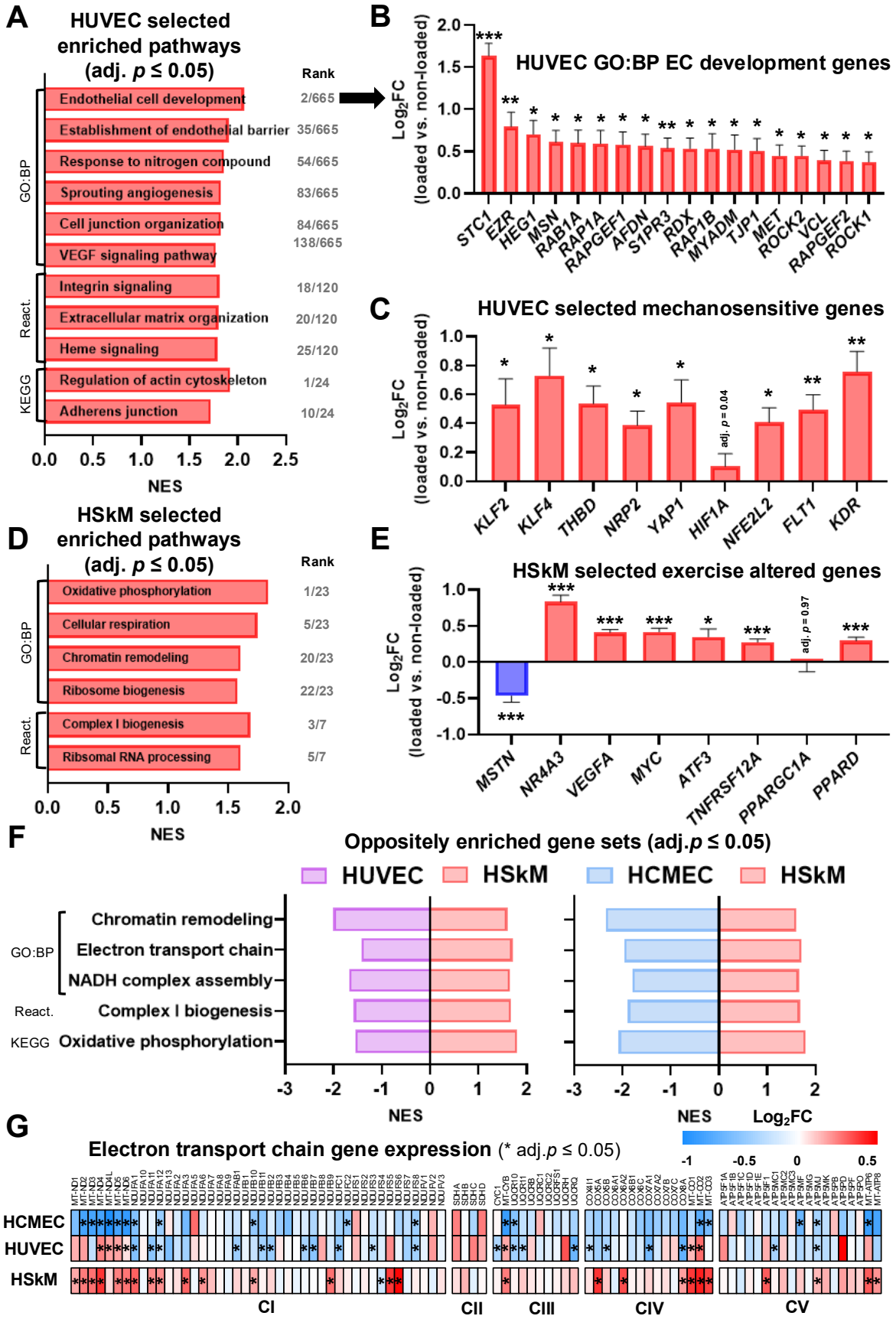
A
HUVEC selected enriched pathways (adj. p ≤ 0.05)
Rank
Endothelial cell development 2/665
Establishment of endothelial barrier 35/665
Response to nitrogen compound 54/665
Sprouting angiogenesis 83/665
Cell junction organization 84/665
VEGF signaling pathway 138/665
Integrin signaling 18/120
Extracellular matrix organization 20/120
Heme signaling 25/120
Regulation of actin cytoskeleton 1/24
Adherens junction 10/24
GO:BP
React.
KEGG
NES
B
HUVEC GO:BP EC development genes
Log2FC (loaded vs. non-loaded)
STC1 EZR HEG1 MSN RAB1A RAP1A RAPGEF1 AFDN S1PR3 RDX RAP1B MYADM TJP1 MET ROCK2 VCL RAPGEF2 ROCK1
C
HUVEC selected mechanosensitive genes
Log2FC (loaded vs. non-loaded)
adj. p = 0.04
KLF2 KLF4 THBD NRP2 YAP1 HIF1A NFE2L2 FLT1 KDR
D
HSkM selected enriched pathways (adj. p ≤ 0.05)
Rank
Oxidative phosphorylation 1/23
Cellular respiration 5/23
Chromatin remodeling 20/23
Ribosome biogenesis 22/23
Complex I biogenesis 3/7
Ribsomal RNA processing 5/7
GO:BP
React.
NES
E
HSkM selected exercise altered genes
Log2FC (loaded vs. non-loaded)
adj. p = 0.97
MSTN NR4A3 VEGFA MYC ATF3 TNFRSF12A PPARGC1A PPARD
F
Oppositely enriched gene sets (adj.p ≤ 0.05)
HUVEC HSkM HCMEC HSkM
GO:BP
Chromatin remodeling
Electron transport chain
NADH complex assembly
React.
Complex I biogenesis
KEGG
Oxidative phosphorylation
NES
NES Log2FC
G
Electron transport chain gene expression (* adj.p ≤ 0.05)
HCMEC
HUVEC
HSkM
CI
CII
CIII
CIV
CV

172

Fig. 2 Transcriptomic changes of endothelial and muscle cells in response to mechanical loading. **A)** Selected positively enriched gene sets in HUVECs from GO:BP, Reactome and KEGG database terms. **B)** Upregulated individual genes in HUVECs in GO:BP *Endothelial cell development* -pathway. **C)** Selected individual mechanosensitive endothelial genes in HUVECs. **D)** Selected positively enriched gene sets in HSkM cells from GO:BP and Reactome database terms. **E)** Selected individual exercise-altered genes in HSkM cells. **F)** Five gene sets from GO:BP, Reactome and KEGG terms, that were significantly downregulated in both endothelial cell lines and upregulated in muscle cells. **G)** Heatmap depicting expression of individual genes in all electron transport chain complexes in response to mechanical loading. NES = Normalized enrichment score. GO:BP = Gene ontology:Biological process. Rank = Rank of gene set by NES in all statistically significant (adj. $p \leq 0.05$) up- or downregulated gene sets in their respective database. Data are presented as mean ± SEM. **adj. $p < 0.05$, **adj. $p < 0.01$, ***adj. $p < 0.001$*

Together, in endothelial cells mechanical loading induced positive enrichment of pathways related to maturation and barrier establishment as well as upregulation of known mechanosensitive genes. In muscle cells mechanical loading upregulated OXPHOS and ribosome biogenesis pathways, as well as changes in typical resistance exercise-regulated genes, suggesting that mechanical loading alone recapitulates several common exercise effects seen *in vivo*. The transcriptomic results clearly demonstrated cell type-specific responses induced by mechanical loading. This was seen especially in the opposite expression of ETC-complex genes, which were downregulated in endothelial cells and upregulated in muscle cells.

Mechanical loading resulted in greater metabolite changes in endothelial cells compared to muscle cells

Next, we compared metabolite changes in HUVECs and HSkM cells in response to mechanical loading. We analyzed a targeted list of intracellular metabolites with UHPLC-MS/MS, and culture media metabolites with non-targeted ^{1}H NMR spectroscopy (Fig. 3A, Supplementary Table S5). In HSkM cells and HUVECs, 3/35 and 11/38 intracellular metabolites were altered in response to mechanical loading, respectively (Fig. 3B). The intracellular metabolite alterations were thus greater in HUVECs than in HSkM cells, which is in line with the transcriptome results. From the extracellular metabolites (conditioned media), 3/29 were altered in HSkM cells, and 2/34 in HUVECs (Fig. 3B).

By comparing conditioned media to the media incubated without cells (i.e., cell-free media), we found that both HUVECs and HSkM cells released acetate into the media in response to mechanical loading (Fig. 3C-D). We also confirmed the acetate release with UHPLC-MS (Supplementary Fig. 3), which identified an even more pronounced acetate release than ^{1}H NMR (Supplementary Fig. 3A-B). In addition, arginine and glutamine levels were greater in the media of loaded HSkM cells and pyruvate levels in the media of loaded HUVECs (Fig. 3C-D).

In muscle cells, intracellular levels of glucose 6-phosphate and phosphocreatine decreased while alanine levels increased in response to mechanical loading (Fig. 3E). In

HUVECs, intracellular levels of phosphoenolpyruvate, fructose 6-phosphate, and α-ketoglutarate decreased while phosphoserine, serine, asparagine, threonine, proline, alanine, acetyl-CoA, and tryptophan levels increased (Fig. 3F). The two mostly increased metabolites were phosphoserine and serine (Fig. 3F), whereas the serine synthesis pathway gene expressions were unaffected (Supplementary Table S1). Proline and α-ketoglutarate were the two most consistently (smallest *p*-values) changed metabolites. The observed increase in proline and decrease in α-ketoglutarate may indicate that proline was synthesized using α-ketoglutarate.

Next, we conducted a metabolite overrepresentation analysis using the significantly altered intracellular metabolites. The overrepresentation analysis of HSkM cells did not yield any significant results because of the low number of altered metabolites. In HUVECs, the most enriched pathways were *Glycine and serine metabolism*, *Glutamate metabolism*, and the *Warburg effect* (Fig. 3G).

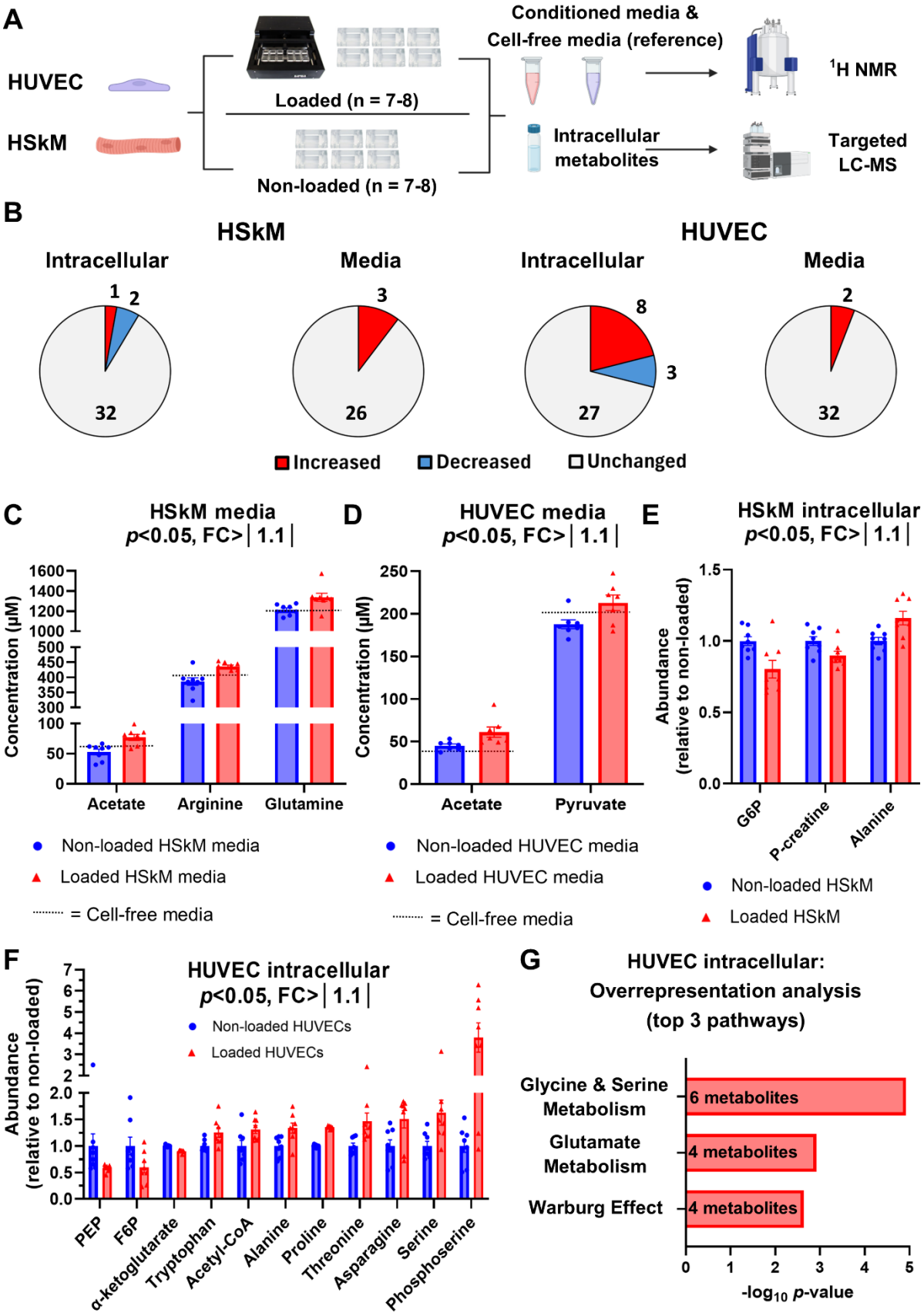

Fig. 3 Intracellular and culture media metabolite changes of human skeletal muscle cells (HSkM) and HUVECs in response to mechanical loading. **A)** Culture media metabolites were analyzed with ¹H NMR spectroscopy, and intracellular metabolites were analyzed using the targeted

UHPLC-MS/MS method. Cells or media from three stretching chambers were pooled for one sample. Also, media incubated without cells (i.e., Cell-free media) was included as an additional reference. **B)** The number of increased, decreased, and unchanged intracellular and culture media metabolites of HSkM cells and HUVECs. **C)** Significantly changed media metabolites of HSkM cells. **D)** Significantly changed media metabolites of HUVECs. **E)** Significantly changed intracellular metabolites in HSkM cells. **F)** Significantly changed intracellular metabolites in HUVECs. **G)** Metabolite overrepresentation analysis using the significantly altered intracellular metabolites of HUVECs. In panel G, the number of metabolites indicates how many significantly altered metabolites from each pathway were detected. Individual values (n = 7-8 per group) are plotted, and data are presented as mean ± SEM. The dashed lines represent the average concentrations in cell-free media samples. P-creatine = Phosphocreatine, G6P = Glucose 6-phosphate, PEP = Phosphoenolpyruvate, F6P = Fructose 6-phosphate

Mechanical loading increased the synthesis of serine, alanine, and proline from glucose in endothelial cells

As serine metabolism was the most highlighted pathway in mechanically loaded HUVECs, and its role in survival and growth has been demonstrated (26), we next conducted dynamic labeling experiments with ^{13}C-(U)-glucose (Fig. 4A) to assess whether the serine synthesis rate is affected by mechanical loading. We found that there were significantly more total (unlabeled + labeled) and newly synthesized serine and phosphoserine at multiple time points after mechanical loading (Fig. 4B-E). This indicates that the serine synthesis was indeed increased in response to mechanical loading in HUVECs. Total serine levels did not change in the media (Fig. 4F) whereas mechanically loaded HUVECs released significantly more labeled serine into the culture media (Fig. 4G), supporting the interpretation that serine synthesis was increased by mechanical loading.

We also assessed the synthesis of alanine, proline, glycine, aspartate, asparagine, glutamine, glutamate, and arginine. We observed more labeled and total alanine and proline in loaded HUVECs and their media (Supplementary Fig. 4A-G), indicating that alanine and proline synthesis were increased together with serine synthesis in response to mechanical loading.

There was significantly less labeled glycine in loaded HUVECs at 3 h and 20 h time points and total glycine at the 0 h time point (Supplementary Fig. 4H-I), but no differences in labeled or total glycine release into media (Supplementary Fig. 4J-K) compared to non-loaded controls. We did not find significant differences in labeled aspartate and glutamate (Supplementary Fig. 5). In the case of asparagine, arginine, and glutamine, ^{13}C-labeled molecules were not detected after isotope natural abundance correction, suggesting that HUVECs did not use glucose to produce these amino acids in these nutritional conditions (Supplementary Table S6). Overall, the results suggest that mechanical loading induces the synthesis of serine, alanine, and proline in endothelial cells.

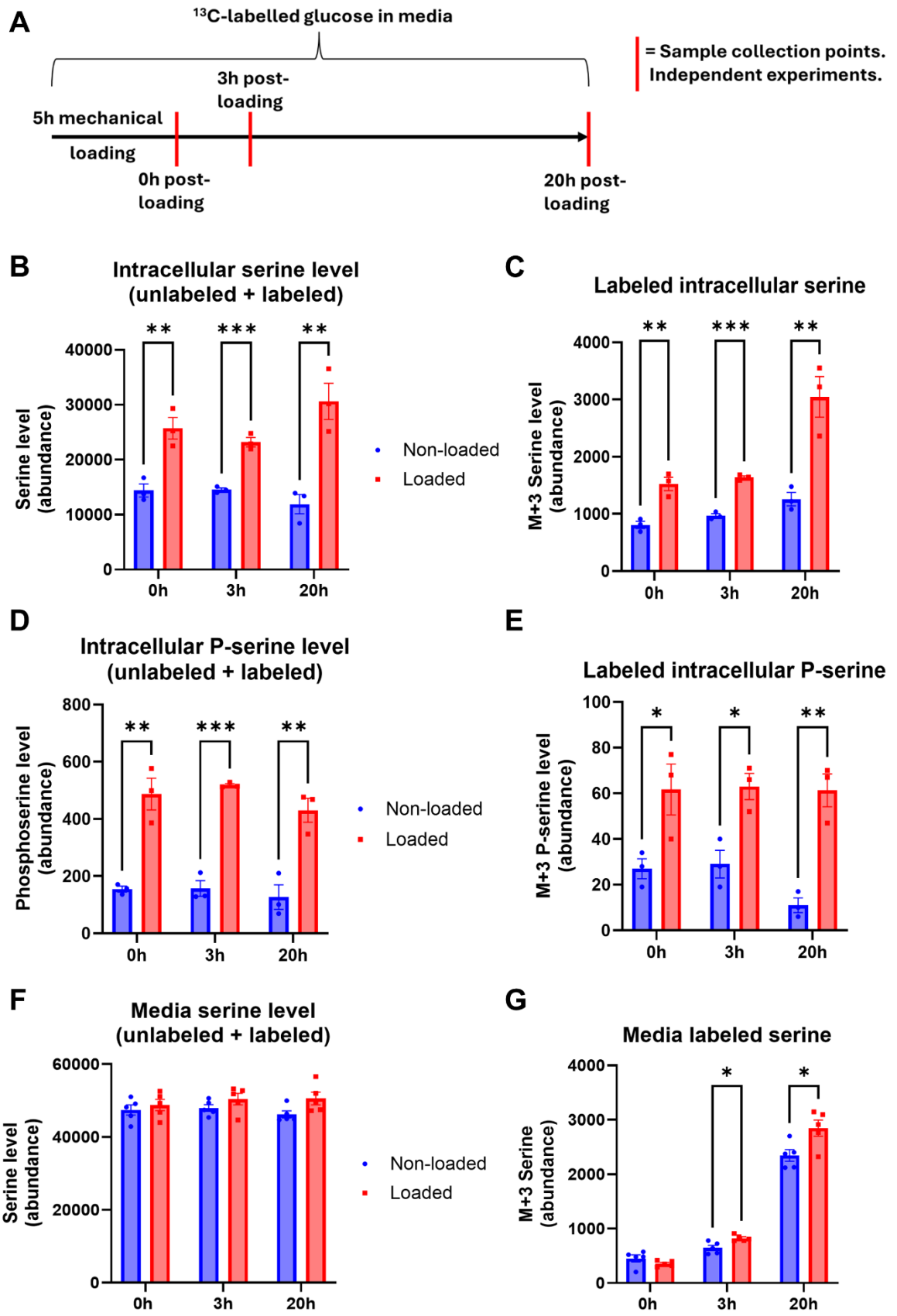

Fig. 4 Mechanical loading increased glucose-derived carbon incorporation into serine and phosphoserine in HUVECs. **A)** A schematic diagram of the time points of the ^{13}C-(U)-glucose experiment. **B)** Total intracellular serine level (unlabeled + labeled). **C)** Newly synthesized (M+3)

serine level. **D)** Total intracellular phosphoserine (P-serine) level (unlabeled + labeled). **E)** Newly synthesized (M+3) phosphoserine level. **F)** Total media (extracellular) serine level (unlabeled + labeled). **G)** Newly synthesized (M+3) media serine level. Sample sizes were n = 3 per group per time point in intracellular analyses and n = 5 in media analyses. Individual values are plotted, and data are presented as mean ± SEM. *$p < 0.05$, **$p < 0.01$, ***$p < 0.001$.

Mechanical loading induces maturation of endothelial cells

Next, we tested whether mechanical loading alters the proliferation of endothelial cells. We found that mechanical loading decreased proliferation of HUVECs, analyzed with both flow cytometry- and microscopy-based assays (Fig. 5A-B), whereas overall protein synthesis was not affected (Fig. 5C). These results, together with the transcriptomic results for endothelial cell development (Fig. 2B), suggest that mechanical loading induces maturation and junctional stability of endothelial cells and inhibits proliferation. To translate our results to an *in vivo* situation, we applied the MetaMEx database (19) to examine whether the *Endothelial Cell Development* -pathway is commonly induced in response to acute aerobic exercise, and indeed we found this to be the case for several of these genes (Supplementary Fig. 6).

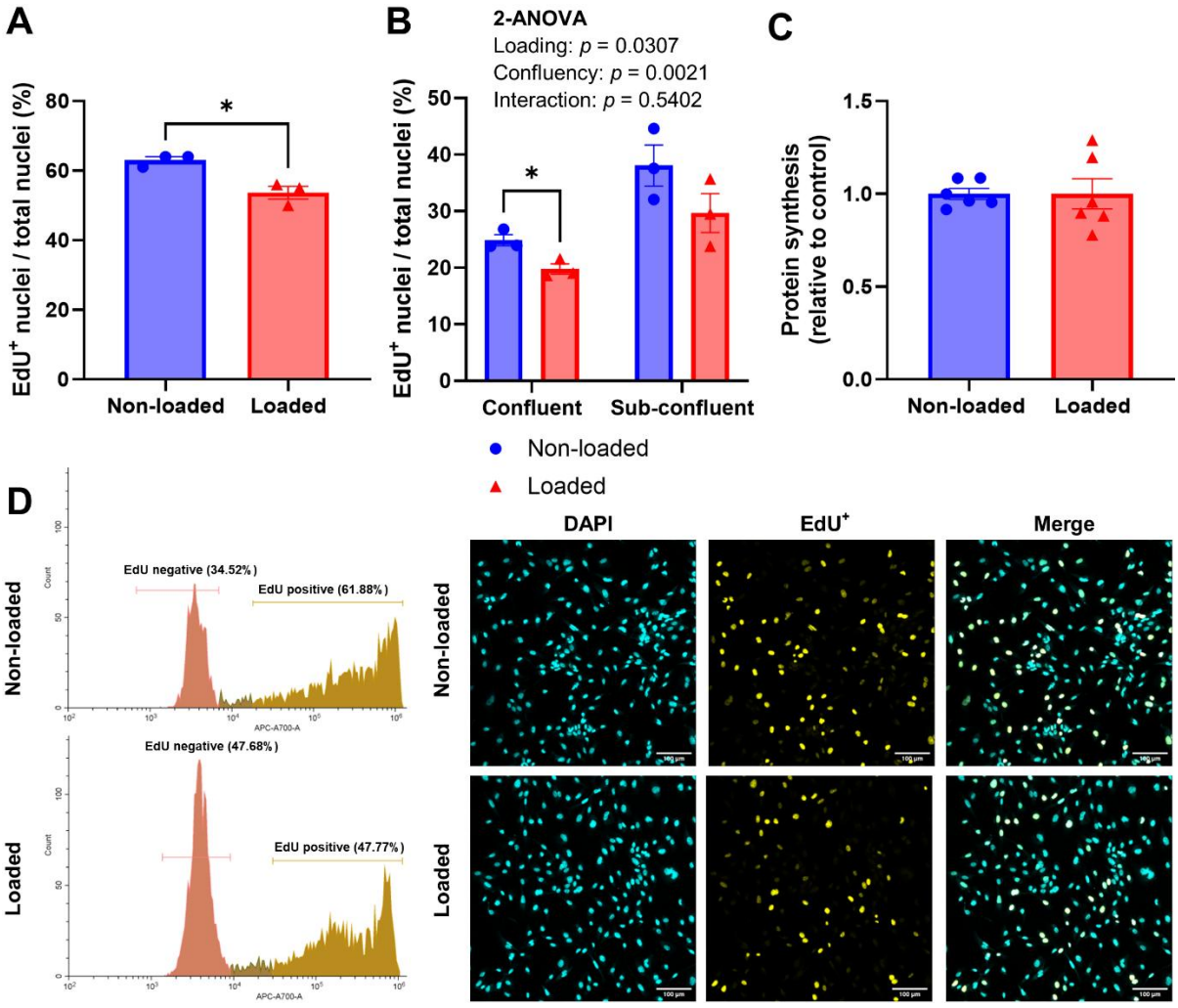

Fig. 5 Effects of mechanical loading on endothelial cell proliferation and protein synthesis. A) EdU-positive cells analyzed with flow cytometry (n = 3). B) EdU-positive cells in confluent and

298 sub-confluent cell densities were analyzed with confocal microscopy (n = 3). C) Protein synthesis
299 assessed by relative ^{14}C-phenylalanine incorporation (n = 6). **D**) Representative flow cytometry
300 histograms showing EdU negative and positive cell populations, and next to them are
301 representative confocal microscopy images showing all nuclei (dapi) and EdU positive nuclei.
302 Data are presented as mean ± SEM, and individual values are plotted when applicable. *$p < 0.05$.
303

304 Serine synthesis pathway enzyme phosphoglycerate dehydrogenase 305 (PHGDH) is critical for endothelial cell anabolism

306 Finally, to extend the previous findings on the role of the serine synthesis pathway in
307 endothelial cells (26), we used a lentiviral vector to overexpress PHGDH, the rate-
308 limiting enzyme of the serine synthesis pathway (Fig. 6A). Overexpression of PHGDH led
309 to a ~10% increase in protein synthesis ($p < 0.01$, Fig. 6A) and a trend for increased
310 proliferation ($p = 0.088$, Fig. 6C) in HUVECs. Next, we used chemical PHGDH inhibitors
311 and evaluated their effects on protein synthesis and proliferation. We discovered that
312 PHGDH inhibitors decreased the protein synthesis and proliferation of HUVECs (Fig. 6D-
313 E) without inducing cell death (Fig. 6F). We also found that the PHGDH inhibitors
314 decreased glucose-derived carbon incorporation into proteins, RNA, and lipids
315 (Supplementary Fig. 7). Overall, these data suggest that the serine synthesis pathway
316 enzyme PHGDH regulates endothelial cell growth, similarly to what we recently showed
317 in muscle cells (27, 28).

318

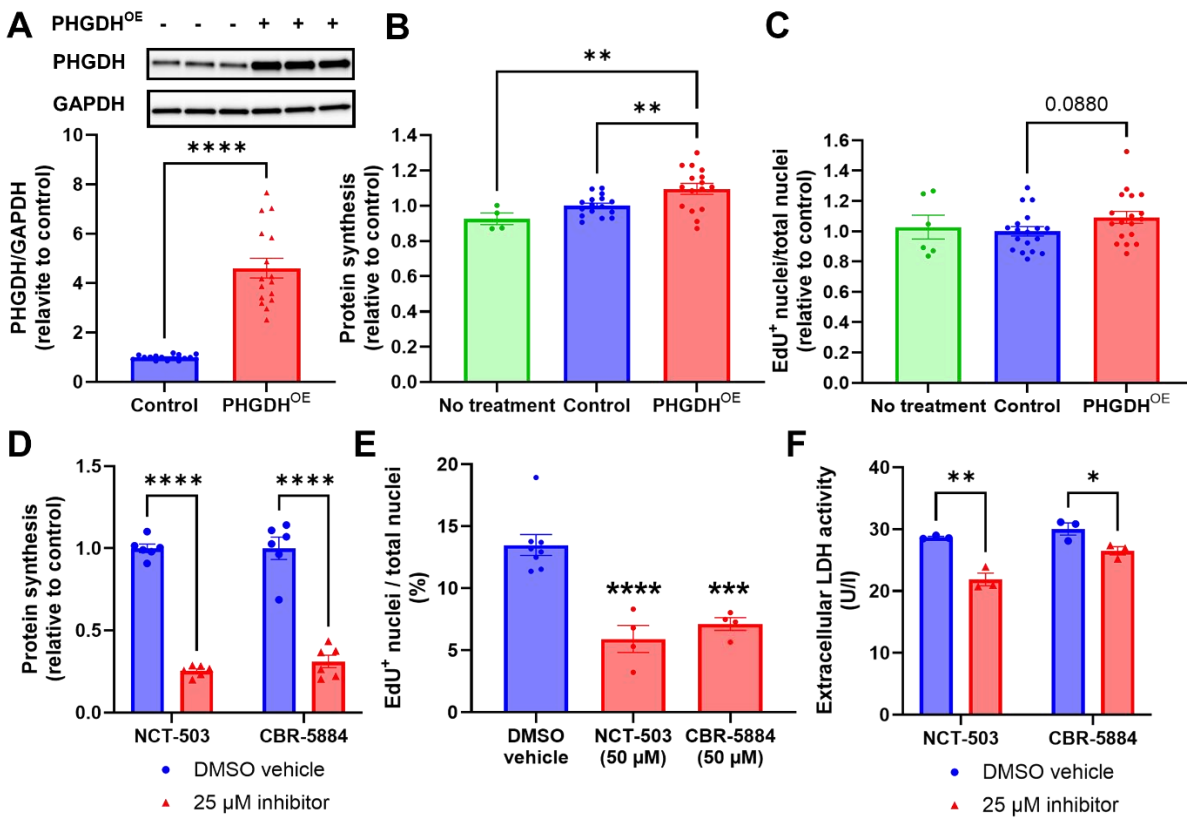

319

320 **Figure 5.** Effects of the serine synthesis pathway enzyme phosphoglycerate dehydrogenase
321 (PHGDH) manipulation on cell proliferation and protein synthesis. **A)** PHGDH level in response

322 to overexpression treatment (n = 16). **B)** Protein synthesis (^{14}C-phenylalanine incorporation into
323 proteins) in response to PHGDH overexpression treatment (n = 16, but in no treatment group n =
324 4). **C)** Cell proliferation in response to PHGDH overexpression treatment (n = 24, but in the no-
325 treatment group n = 6). **D)** protein synthesis (relative ^{14}C-valine incorporation into proteins) in
326 response to PHGDH inhibitors NCT-503 and CBR-5884 (n = 6). **E)** PHGDH inhibitors decreased
327 the proliferation of HUVECs, as assessed by EdU analysis. The groups were statistically
328 compared only to the DMSO vehicle control (n = 8 in the DMSO control group and n = 4 in the
329 inhibitor groups). **F)** PHGDH inhibitors did not induce cell death according to the lactate
330 dehydrogenase (LDH) activity measured from conditioned media (i.e., increased LDH activity
331 would indicate membrane damage and cell death) (n = 3). Individual values are plotted, and data
332 are presented as mean ± SEM. *$p < 0.05$, **$p < 0.01$, ***$p < 0.001$, **** $p < 0.0001$.
333

334 Discussion

335 In this study, we unraveled the effects of mechanical loading on skeletal muscle and
336 endothelial cells and identified both shared and cell type-specific responses. Notably,
337 both muscle and endothelial cells significantly increased acetate release into the media
338 and induced gene expression changes typically observed after exercise. However,
339 transcriptomic responses exhibited several contrasting patterns in endothelial and
340 muscle cells. Most strikingly, OXPHOS and electron transport chain (ETC) genes were
341 upregulated in muscle cells but downregulated in endothelial cells. Furthermore,
342 endothelial cells demonstrated more pronounced metabolic responses, particularly in
343 amino acid metabolism. In response to mechanical loading, endothelial cells decreased
344 proliferation and upregulated expression of genes related to maturation and junctional
345 stability. Furthermore, using a ^{13}C-(U)-glucose tracer, we demonstrated that mechanical
346 loading enhanced glucose-derived serine synthesis in endothelial cells. Overexpression
347 of the serine synthesis enzyme PHGDH promoted protein synthesis of endothelial cells,
348 whereas PHGDH inhibitors decreased proliferation and anabolic activity, highlighting the
349 role of de novo serine synthesis from glucose in endothelial cell growth.

350 Both muscle and endothelial cells released acetate into the media in response to
351 mechanical loading, which was observed with two different analysis methods.
352 Previously, we found that electrically evoked myotube contractions also induced acetate
353 release from murine myotubes (29). In humans, it has been found that acetate is
354 released into the bloodstream (30) and urine (31) after exercise. Moreover, serum
355 acetate concentrations have been found to be greater in physically active individuals
356 compared to inactive individuals (32). Therefore, acetate could act as a possible exerkine
357 (i.e. a signaling molecule released in response to exercise) released by not only muscle
358 cells but also endothelial cells. One of the most relevant functions of acetate is acting as
359 an immunomodulator and promoter of T-cell effector function and regulating
360 differentiation of $CD4^+$ T-cell helper cells (33–35). This may partly explain the effects of
361 exercise in enhancing immune system function and increasing $CD4^+$ T-helper cell count
362 in humans (36). This is particularly interesting, as factors secreted by $CD4^+$ T-cells seem
363 to be important in angiogenesis, myogenesis, and muscle regeneration (37, 38). In
364 addition, the potential source of acetate after mechanical loading is interesting, as

acetate can be produced from (A) acetyl-CoA by certain acyl-CoA thioesterases (39), (B) from pyruvate by ketoacid dehydrogenases and reactive oxygen species (40), and (C) by deacetylation of proteins (41). Of these, at least reactive oxygen species production is induced in muscle by exercise (42). Thus, acetate's possible role as an exerkine and its links to the immune system or other human physiological systems should be studied further.

Endothelial cells and muscle cells also demonstrated different and even opposite transcriptomic responses to mechanical loading, most prominently in OXPHOS-related pathways, and specifically in ETC complex genes. In endothelial cells the expression of these genes was downregulated, and it has previously been shown that they primarily rely on glycolysis for ATP production despite having access to oxygen, and that vessel sprouting *in vitro* is regulated by glycolysis (43). OXPHOS-related genes were on the other hand upregulated in muscle cells, and skeletal muscle is known to upregulate mitochondrial biogenesis and oxidative respiration in response to physiological stress, such as exercise (15). One of the well-known mechanisms regulating these exercise adaptations is the AMPK-PGC1α pathway (23). In our study, although PGC1α gene expression was unchanged in muscle cells, we did observe an increase in *PPARD* expression after mechanical loading. PPARD is upstream of PGC1α (24) and has been linked to enhanced oxidative metabolism in skeletal muscle (25). Furthermore, muscle cells also demonstrated an upregulation of the *NR4A3, ATF3, and TNFRSF12A*, which have been shown to belong to the five most upregulated genes in response to resistance exercise (19). For example, *NR4A3* is essential in glucose metabolism and anabolism, such as ribosome biogenesis in primary muscle cells (20). In line with the upregulation of *NR4A3*, we also observed increases in the *ribosome biogenesis* GO:BP pathway after mechanical loading, which is a known response to resistance training (44). Moreover, we saw a decrease in myostatin (*MSTN*) expression in muscle cells, which is a common response after a single bout of resistance exercise (21, 22). These results demonstrate that mechanical loading of human skeletal muscle cells recapitulates several of the common effects of exercise seen *in vivo*.

In endothelial cells, transcriptomic results showed that mechanical loading induced upregulation of genes related to endothelial cell development, migration, cell-cell junctions, and endothelial barrier integrity. Many of the endothelial cell development genes were also found to increase in response to acute aerobic exercise in human skeletal muscle tissue, which is known to be highly vascularized (1, 2, 19). Furthermore, our results showed upregulation of mechanosensitive genes commonly associated with an atheroprotective endothelial phenotype, which are typically induced by flow-mediated mechanical stress (16–18). Our findings point out that a similar effect was seen after cyclic stretching, which is comparable to skeletal muscle movement. We also found that genes related to VEGF response, including VEGF receptors 1 & 2 (*FLT1 & KDR*), were upregulated in endothelial cells. Related to these, *VEGFA* expression was also increased in mechanically loaded muscle cells, and it has been hypothesized that skeletal muscle stem cells recruit endothelial cells via VEGF-A expression and this interaction is important for muscle stem cell self-renewal (45). Recently, a study

408 investigating acute endothelial-specific transcriptional responses in mouse skeletal
409 muscle found that exercise induced activation of pathways related to endothelial cell
410 development, differentiation, and migration, as well as VEGF response (46), which align
411 well with our results and validates that mechanical loading of endothelial cells
412 recapitulates effects of exercise *in vivo*.

413 In endothelial cells, we observed upregulation of heme signaling- and endothelial cell
414 maturation-related genes in response to mechanical loading. Further, ^{13}C-glucose
415 tracing analysis revealed that the abundance and synthesis of serine increased after
416 mechanical loading. Moreover, the overexpression of the serine-synthesizing enzyme
417 PHGDH increased protein synthesis, while commonly used non-competitive PHGDH
418 inhibitors decreased proliferation, protein synthesis, and glucose utilization for
419 anabolism. This is similar to what we recently demonstrated in muscle cells (27, 28).
420 Loss of PHGDH has previously been shown to cause lethal defects in angiogenesis in
421 mice and knockdown of PHGDH impairs endothelial cell proliferation (26). Moreover,
422 PHGDH has been highlighted as essential for the regulation of heme production in
423 endothelial cells (26), and hemin (oxidized heme) supplementation promotes
424 differentiation of endothelial progenitor cells (47). These results suggest that
425 mechanical stimuli/exercise, the serine synthesis pathway, heme signaling, and
426 endothelial cell maturation may be interconnected.

427 **Strengths and limitations**

428 We used two different human endothelial cell types and primary human skeletal muscle
429 cells. The loading induced several common exercise-induced and mechanosensitive
430 genes, suggesting an external validity of the exercise-on-a-dish model. Moreover, several
431 of the transcriptomic responses to mechanical loading were similar between the two
432 endothelial cell types (HUVEC and HCMEC), suggesting that many of the changes can be
433 applied to endothelial cells in general. We also replicated the main metabolite and
434 proliferation results with different methods. For example, acetate release was observed
435 with both ^{1}H NMR spectroscopy and UHPLC-MS, and the decrease in proliferation was
436 determined with microscopy- and flow-cytometry-based analyses. In addition, the
437 increased serine, alanine, and proline content and synthesis were detected by targeted
438 metabolomics and isotopic tracing from multiple time points.

439 The study also has limitations. We conducted the experiments with monolayers of cells
440 (i.e., two-dimensionally), and therefore, myotubes were not aligned unidirectionally
441 while the mechanical loading was unidirectional. In contrast, smaller endothelial cells
442 could change their alignment against the direction of stretch. This difference in the ability
443 to change alignment may in part explain why we detected fewer molecular changes in
444 myotubes compared to endothelial cells, although myotubes also recapitulated several
445 exercise responses. Overall, the data suggest that the mechanical loading model for two-
446 dimensionally cultured cells is especially suitable for endothelial cells, which also grow
447 in monolayers *in vivo*, while myotubes may need to be loaded three-dimensionally to
448 sufficiently mimic exercise in future studies. The potential importance of the mechanical

449 loading and serine synthesis pathway for improved vascular function should be studied
450 *in vivo* in further studies.

451 **Conclusion**

452 Mechanical loading induces both common and highly cell type-specific transcriptomic
453 and metabolomic responses in endothelial and skeletal muscle cells. In general, several
454 of the effects recapitulated what is observed *in vivo* after exercise. Both endothelial and
455 muscle cells released acetate in response to mechanical loading, and therefore
456 acetate's potential role as an exerkine could be an interesting topic for future studies.
457 The responses to mechanical loading were larger in endothelial cells, revealing
458 increased serine synthesis and upregulation of endothelial cell development as one of
459 the main responses. These results highlight that mechanical stimulus, serine synthesis,
460 and endothelial cell maturation may be interconnected.

461

462 Materials and methods

463 Endothelial and muscle cells

464 We used human umbilical vein endothelial cells (HUVEC, Cat# C-12200, PromoCell),
465 human cardiac microvascular endothelial cells (HCMEC, Cat# C-12285, PromoCell),
466 and primary human skeletal muscle (HSkM) cells. The latter were obtained as previously
467 (27) from two healthy 25-34-year-old volunteers (1 male and 1 female). Vastus lateralis
468 muscle biopsies were obtained under local anesthesia with the Bergström biopsy
469 needle. The human study (48) was conducted in accordance with the Declaration of
470 Helsinki and was approved as part of a larger TraDeRe-study by the Ethics Committee of
471 the University of Jyväskylä (857/13.00.04.00/2021). All participants provided written
472 informed consent for inclusion prior to participating in the study.

473 Cell culture

474 The HUVEC and HCMEC cells were cultured in endothelial cell growth medium (EGM)
475 (Cat# C-22010, PromoCell) supplemented with EGM SupplementMix (Cat# C-39215,
476 PromoCell) and 1% (vol/vol) of 1000 U/ml penicillin-streptomycin (P/S, Cat# 11548876,
477 Gibco). HSkM cells were cultured in growth medium (GM) consisting of high glucose (4.5
478 g/l) Dulbecco's Modified Eagle Medium (DMEM, Cat# 10313021, Gibco) supplemented
479 with 20% (vol/vol) fetal bovine serum (FBS, Cat# 10270106, Gibco), 1% (vol/vol) of 1000
480 U/ml P/S and 1% (vol/vol) 200 mM L-glutamine (Cat# 11500626, Gibco).

481 After reaching over 80% confluency in culture flasks, the cells were seeded (~20,000
482 cells/cm^2) on polydimethylsiloxane (PDMS) chambers (Cat# STB-CH-04, STREX). PDMS
483 chambers were pre-coated with FBS for 24 h and with 0.2% gelatin for an additional 24 h.
484 The PDMS chambers were placed in 150 mm diameter Petri dishes, two chambers per
485 dish. Cells were grown on PDMS chambers until reaching over 80% confluency. After
486 that, HUVEC and HCMEC cells were mechanically loaded, as described in the next

487 section. In the case of HSkM cells, at 80% confluency the GM was replaced with
488 differentiation medium (DM) containing high glucose DMEM, 2% (vol/vol) horse serum
489 (HS, Cat# 26050088, Thermo Fisher Scientific), 1% P/S, 1% L-glutamine and 1% (vol/vol)
490 Insulin-Transferrin-Selenium-X supplement (ITS-X, Cat# 51500056, Gibco). To induce
491 myoblast fusion into myotubes, the cells were cultured in DM for 4-5 days and DM was
492 changed every 48 h. Cells were cultured at 37 ℃ in a 5% CO_2 atmosphere all the time.

493 Mechanical loading set-up

494 Mechanical loading of cultured cells was achieved with a commercial cell culture pacing
495 system (C-Pace EM 100, IonOptix) paired with a motor-powered mechanical stimulation
496 unit (C-Stretch 100, IonOptix). The C-Stretch mechanical stimulation unit consists of a
497 motor-driven tray that causes uniaxial elongation of the PDMS chambers inserted in the
498 device and exposes cells, that are attached to the bottom of the chamber, to mechanical
499 load.

500 As mentioned, cells were seeded onto 12 PDMS chambers for each stretch experiment,
501 with 6 chambers loaded into the C-Stretch unit in series, and 6 chambers left as static
502 controls. The stretch unit was thoroughly cleaned with 70% EtOH before use. Fresh
503 media was changed for all chambers prior to starting the experiment. The stretch unit
504 was then placed in an incubator with conditions of 37 ℃ and 5% CO_2 atmosphere along
505 with the 6 control chambers. A cyclic mechanical stretch with a frequency of 1 Hz and
506 12% elongation was applied for 5 h. For each one-second cycle, a trapezoidal waveform
507 of 0.4 s stretch, 0.1 s hold, 0.4 s return, and 0.1 s hold, was used to keep the velocity of
508 the deformation of the silicone chamber at a moderate speed.

509 Lactate dehydrogenase activity assay

510 Lactate dehydrogenase activity (LDH) was measured from conditioned media as an
511 indicator of possible membrane damage and cell death (49). The analysis was
512 performed as previously (27) using an LDH Activity Assay Kit (Cat# 981906, Thermo
513 Fisher Scientific).

514 RNA extraction and analyses

515 RNA isolation, library preparation and sequencing

516 RNA was extracted using a commercial column-based RNA isolation kit (NucleoSpin®
517 RNA, Cat# 740955.250, Macherey-Nagel) immediately after the 5-hour mechanical
518 loading. The PDMS chambers were washed with PBS, and cells were lysed by pipetting
519 back and forth vigorously with lysis solution (350 µl of guanidium thiocyanate lysis buffer
520 + 3.5 µl of β-mercaptoethanol). Extraction was then continued according to the kit's
521 instructions. An additional centrifugation step of 30 s at 11 000 g was included at the end
522 to ensure complete removal of the wash buffer. Bound RNA was then eluted into a
523 volume of 60 µl of RNase-free water. The collected elution was then aliquoted and
524 samples were immediately transferred to -80 °C. RNA quality control, library preparation
525 and sample sequencing were performed at Novogene (Cambridge, United Kingdom),

526 utilizing an Illumina NovaSeq 6000 platform, producing 150bp paired-end reads. Filtering
527 of raw sequence data was also conducted by Novogene in the following way: (1)
528 removing reads containing adapters, (2) removing reads containing >10% of unsolvable
529 bases and (3) removing reads containing >50% of low quality bases (Qphred ≤ 5). Filtered
530 RNA sequencing data is available in the Gene Expression Omnibus (GEO) data repository
531 (accession number: GSE288064).

532 Read alignment, normalization and filtering

533 Reads were aligned to the human genome (build GRCh38.95) using the Bowtie2 software
534 (50), with alignment rates >80% for all the samples. The aligned and mapped reads were
535 later annotated and quantified using the Rsubread package in R/Bioconductor software
536 (51), with the human GRCh38.110 genome build as annotation reference. The obtained
537 gene counts were transformed to counts-per-million (CPM) using the edgeR package in
538 the R/Bioconductor software (52). Genes with a CPM < 1 in three samples or more in
539 each group (50%), were subsequently filtered out as described in (53). The resulting
540 expression data were finally normalized using the trimmed mean of M-values (TMM)
541 algorithm (54).

542 Differential gene expression and pathway analyses

543 Differential gene expression (DGE) analyses were implemented through the
544 R/Bioconductor limma-voom pipeline (55). The voom-function of the limma package
545 was initially executed to format the data appropriately (56), after which empirical
546 Bayesian statistics were computed to rank genes based on their evidence for differential
547 expression. To account for type I errors induced by multiple testing, the Benjamini-
548 Hochberg method was used to adjust the tests' *p*-values, retrieving an adjusted *p*-value
549 (adj. *p*). Genes with a $\log_2$FC ≥ 0.5 and adj. $p \leq 0.05$ were regarded as differentially
550 expressed. For subsequent Gene Set Enrichment Analysis (GSEA) genes were ranked in
551 an unbiased way by multiplying the $\log_2$FC by the -log10 of the adj. *p* to consider both the
552 magnitude and consistency of the change in gene expression. GSEA was performed with
553 the clusterProfiler R-package (57) with Gene Ontology: Biological Process (GO:BP),
554 Reactome, and the Kyoto Encyclopedia of Genes and Genomes (KEGG) serving as
555 reference databases. Ontologies and pathways were considered significantly enriched if
556 their corresponding tests yielded an adj. p-value <0.05. In addition, gene set
557 overrepresentation analysis (ORA) of the significantly up- or downregulated genes
558 ($\log_2$FC ≥ 0.5 & adj. $p \leq 0.05$) was conducted using the ShinyGO web-application v0.81
559 (https://bioinformatics.sdstate.edu/go/) (58) from GO:BP pathways. Pathway minimum
560 size was set to 2 and maximum to 5000 and the FDR cutoff for significant pathway
561 enrichment was set to 0.05. All analyses implemented in R/Bioconductor included the
562 core software version 4.3.1 with the R-studio interface version 2024.04.2.

563 Meta-analysis of skeletal muscle response to exercise (MetaMEx)

564 We examined gene expression of the *Endothelial cell development* pathway
565 (GO:0001885, 72 genes, list checked on 10.06.2025) in response to acute aerobic
566 exercise using the MetaMEx browser-based tool

567 (https://www.metamex.eu/app/metamex) (19). All the other settings were kept as a
568 default, except that only the healthy population was included.

569 Metabolite extraction and analyses

570 ^{1}H NMR spectroscopy metabolomics

571 Metabolites from the media samples were extracted as previously (27, 29). Cell-free
572 medium samples were also included as a reference to assess the uptake and release of
573 metabolites. Dried samples were reconstituted with 200 µL of sodium phosphate buffer
574 (150 mM, pH = 7.4) in 99.8% deuterium oxide (Acros Organic; Thermo Fisher Scientific)
575 containing 0.5 mM 3-(trimethylsilyl)propanesulfonic-d_6 acid sodium salt (DSS-d_6; IS-2
576 Internal Standard, Chenomx Inc.) and transferred to round-bottom 3-mm OD NMR tubes
577 (Cat# 341-PP-7, Wilmad). Data collection was carried out at 25 °C using the Bruker
578 AVANCE III HD NMR spectrometer, operating at 800 MHz ^{1}H frequency equipped with a
579 cryogenically cooled ^{1}H, ^{13}C, ^{15}N triple-resonance probe head (Bruker Corporation). The
580 ^{1}H nuclear magnetic resonance (^{1}H NMR) spectra were collected as previously described
581 (29). ^{1}H NMR spectra were processed, and metabolites were identified and quantified
582 with the Chenomx 10.0 software (Chenomx).

583 UHPLC-MS/MS targeted metabolomics

584 Intracellular metabolites were collected and extracted as previously (27) with minor
585 modifications. In brief, 200 µL of ice-cold 80% methanol was added to each stretching
586 chamber, and metabolites from three chambers were pooled for one sample. Dried
587 samples were reconstituted with 40 µl of 50-50 acetonitrile-water mixture (vol/vol)
588 before analysis. Metabolites were analyzed as previously (27). Briefly, metabolites were
589 separated with an Atlantis Premier BEH Z-HILIC UHPLC column (1.7 µm, 2.1 x 100 mm)
590 which was used with an Agilent 1290 Infinity ultra-high-performance liquid
591 chromatography (UHPLC) system. *Mobile phase A* was 15 mM ammonium bicarbonate
592 (pH = 9.0) in water, and *mobile phase B* was 15 mM ammonium bicarbonate (pH = 9.0) in
593 90% acetonitrile-10% water. The flow rate was 0.7 mL/min, the column oven
594 temperature was 40 °C, and the injection volume was 3 µl. The following gradient elution
595 was used: the initial concentration of 90% *B* was held for 1 min and then was linearly
596 decreased to 65% *B* over the next 5 min and was held for 1 min at 65% *B*. Then *B*% was
597 increased to 90% over the next 1 min and was held 2 min at 90% *B* before next injection.
598 The UHPLC system was coupled with an Agilent 6460 triple quadrupole mass
599 spectrometer operated with dynamic multiple reaction monitoring mode (dMRM) as
600 previously described (27). A mixture of target metabolites (concentrations between 10
601 and 50 µM) was injected eight times at the beginning of the analysis and after every 6 to
602 8 samples for quality control and metabolite identification purposes.

603 Acetate was analyzed from media samples using the above-described chromatographic
604 method and the UHPLC-MS instrument which was operated on negative polarization. For
605 acetate, selected ion monitoring [e.g., pseudo-MRM (59)] of *m/z* 59 was done. The
606 following parameters were used for the selected ion monitoring experiment: fragmentor:
607 80; collision energy: 1; cell accelerator voltage: 4. The other ion source parameters were

608 the same as previously reported (27). Retention time and linearity of the signal were
609 tested using 10, 20, 40, 80, and 160 μM acetate standards that were prepared using
610 sodium acetate (Cat# 106268, Merck). The acetate standard was also used for a spike-in
611 experiment.

612 Batch correction, normalization, and statistical analyses of metabolomics
613 data

614 Targeted UHPLC-MS/MS data and ^{1}H NMR data were measured within two batches and
615 therefore, they were batch effect corrected using the EigenMS method on the
616 MetaboAnalyst 6.0 platform (https://www.metaboanalyst.ca/). In the case of UHPLC-
617 MS/MS, data collected with negative and positive modes were separately batch-
618 corrected before combining the data. Single missing values within different groups were
619 replaced with 1/5 of the minimum detected values. Metabolite
620 concentrations/abundances were $\log_2$ transformed for statistical testing with the
621 Student's t-test with significance set at $p < 0.05$ and fold change > I1.1I.

622 Metabolite overrepresentation analysis

623 MetaboAnalyst 6.0 platform was used for the metabolite overrepresentation analysis.
624 Names of the significantly altered metabolites were uploaded. Default settings were
625 used (SMPDB pathway and '*Only use metabolites sets containing at least 2 entries*'
626 option were used).

627 ^{13}C-glucose labeling experiments and analyses

628 Glucose-free and phenol red-free endothelial cell medium (Cat# H1168GPF, Cell
629 Biologics) medium including the medium kit's supplements, was supplemented with 5.5
630 mM U-$^{13}C_6$-D-glucose (Cat# CLM-1396-1, Cambridge Isotope Laboratories, isotopic
631 purity 99%). This medium was changed to the cells just before the initiation of the
632 experiment. Intracellular metabolites were extracted with the same protocol as for
633 targeted UHPLC-MS/MS metabolomics, but this time two chambers were pooled instead
634 of three. Media metabolites were extracted with the same protocol as for ^{1}H NMR
635 metabolomics described above, except now 100 μl of media from each chamber was
636 mixed with 200 μl of methanol. Intracellular and medium metabolites were reconstituted
637 into 45 μl and 400 μl of 50-50 acetonitrile-water solution, respectively. Pooled quality
638 control (QC) samples were prepared by transferring a small aliquot of each sample into
639 a vial (separate QC samples for intracellular and medium metabolites). Selected amino
640 acids were analyzed with the same method as in targeted UHPLC-MS/MS metabolomics
641 described above but the MRM transitions were modified (Supplementary Table S7),
642 allowing analysis of the isotopomers of the selected amino acids. The data was
643 processed and integrated with MRMPROBS_v.3.66 software (60). Phosphoserine and
644 glycine were processed and integrated with Agilent Qualitative Navigator B.08.00
645 software because of their lower abundance. Isotope natural abundances were corrected
646 with IsoCor 2.2.2 software (61) as earlier reported (62).

Chemical inhibitors

For chemical inhibitor experiments, two different PHGDH inhibitors, NCT-503 (Cat# HY-101966) and CBR-5884 (Cat# HY-100012), were obtained from MedChemExpress. Inhibitor stock solutions were prepared in DMSO, and DMSO was also used as vehicle control. The inhibitors were used in concentrations of 25 or 50 µM, as previously used for different cell types (27, 63–65). Further details of inhibitor experiments are described in the next two sections.

Cell proliferation analysis with EdU labeling

Effects of chemical inhibitors (see the section above) on cell division capacity were evaluated using a Click-iT EdU imaging kit (Cat# C10338, Invitrogen). HUVEC cells were plated onto a 96-well plate in Endothelial cell GM and let to grow in subconfluent culture for 24 h. Exposures were added to the wells, four parallel wells for each condition, and eight parallel wells for the control condition (DMSO vehicle). After 20 h incubation of exposures, 5-ethynyl-20-deoxyuridine (EdU) was added for 4 h. Cells were fixed with 4% PFA for 15 min, washed with 3% bovine serum albumin (BSA) in PBS, and permeabilized with 0.5% Triton X-100 in PBS for 20 min RT, and the Click reaction was done according to the manufacturer's instructions. Before imaging, DAPI (0.5 µg/ml) was added to visualize all nuclei. Cells were imaged using a Nikon A1R confocal microscope. The microscope was automated to find optimal focus in each well, image every well, and take 2-9 views per well so that at least 300 nuclei were imaged. Detected nuclei (all nuclei + EdU-stained nuclei) were analyzed using an in-house built Fiji script (https://github.com/seiryoku-zenyo/simple_ratio_DAPIvsPositive-nuclei/tree/main). Shortly, image data was segmented using a deep learning algorithm, separately for DAPI-positive nuclei and EdU-positive nuclei. Next, the ratio between DAPI and EdU nuclei was counted. The data is presented as a fraction (%) of EdU-positive nuclei out of total (DAPI) nuclei.

Click-iT EdU imaging kit (Cat# C10339, Invitrogen) was also used to determine the effect of PHGDH overexpression on HUVEC proliferation. Cells were cultured on 13 mm diameter coverslips (10 000 cell/cm^2) coated with 0.2% gelatin for 24 h, after which cells were incubated with EdU labeling solution for 5 h. Cells were fixed, washed, and permeabilized as above. Click reaction buffer was prepared as described by the manufacturer, added to the cells, and incubated for 30 min protected from light. DAPI (0.5 µg/ml) was used to detect all the nuclei. Cells were imaged with a confocal microscope (Zeiss LSM700) and the number of stained nuclei was calculated manually with Fiji. The data is presented as a fraction (%) of EdU-positive nuclei out of total (DAPI) nuclei.

Effects of mechanical loading on HUVEC proliferation were assessed both by microscopy and flow cytometry. For both analyses, the cells were mechanically loaded as described earlier and incubated in EdU labeling solution during the mechanical loading (5h), plus an additional 2h after cessation of the loading period. For the microscopy analysis, the cells were treated and imaged as above, directly on the PDMS

688 chambers. Quantification of EdU-positive nuclei was performed with the
689 aforementioned in-house-built Fiji script. The Click-iT™ EdU Alexa Fluor™ 647 Flow
690 Cytometry Assay Kit (Cat# C10424, Invitrogen) was used for the flow-cytometry analysis.
691 HUVECs were detached after the EdU incubation, and two PDMS chambers were pooled
692 as one sample to ensure a sufficient number of cells for the flow cytometer. Fixing,
693 washing, and staining of the cells were performed following the kit instructions.
694 EdU analysis was performed with CytoFLEX S Flow Cytometer using red 638 nm laser
695 with 712/25 BandPass filter and Cytexpert software 2.4.0.28. Quality control was
696 performed using CytoFLEX Ready-To-Use Daily QC Fluorospheres, and an unstained
697 HUVEC pool was used as a compensation control. 10000 datapoints were collected. Cell
698 debris and determination of singlets with SSC and FSC were performed. Analysis of
699 EdU^+ and EdU^- signals was done utilizing histograms.

700 Carbon-14 labeling

701 For evaluation of relative protein synthesis and glucose-incorporation the following
702 radioisotope tracers were used: ^{14}C-[1]-L-phenylalanine (0.1 mCi/mL, Cat#
703 NEC859S050UC, Revvity); ^{14}C-[U]-L-valine (271.0 µCi/mmol, Cat# NEC291EU050UC,
704 PerkinElmer); and ^{14}C-[U]-glucose (0.2 mCi/mL, Cat# NEC042V250UC, PerkinElmer).
705 Only one tracer per experiment was used, and the dilution of the tracers was 1 µL/mL
706 (vol/vol) in the culture media. Two milliliters of culture media were used per well of a 6-
707 well plate, and one milliliter per stretching chamber

708 HUVECs for PHGDH inhibitor experiments were seeded onto 0.2% gelatin-coated 6-well
709 plates at a density of 12,500 cells/cm^2. The cell population was expanded for 2 days, and
710 the inhibition experiments were initiated by changing the media to experimental media
711 containing 25 µM of inhibitor and a radioisotope tracer. After incubating cells for 48 h
712 with inhibitor and tracer, proteins, RNA, and lipids were extracted, and liquid scintillation
713 counting was conducted as previously (27). When protein synthesis was measured
714 during and after mechanical loading, tracer was added to the medium just before the
715 initiation of the 5 h mechanical loading. After the loading, HUVECs were incubated for an
716 additional 20 h in the medium, and then proteins were extracted.

717 PHGDH overexpression

718 The PHGDH overexpression construct pLJM5-WT PHGDH was a gift from David Sabatini
719 (Addgene plasmid #83901; http://n2t.net/addgene:83901; RRID: Addgene_83901) (66).
720 Lentivirus particles were prepared and distributed by Biomedicum Virus Core facility
721 supported by HiLIFE and the Faculty of Medicine, University of Helsinki, and Biocenter
722 Finland. The control construct, clone SHC002 (Scrambled shRNA in pLKO.1) was from
723 Sigma Aldrich MISSION shRNA library, distributed by Genome Biology Unit core facility
724 supported by HiLIFE and the Faculty of Medicine, University of Helsinki, and Biocenter
725 Finland. The Biomedicum Virus Core facility also determined the p24 capsid protein
726 concentration with an enzyme-linked immunosorbent assay (ELISA). p24 concentrations
727 were used to calculate the number of virus particles needed for transduction (1 pg of p24
728 = 100 transducing units).

HUVECs were cultured in T75 flasks. After reaching 50% confluence, 10 ml of medium containing lentiviruses (MOI = 50) and polybrene (5 µg/ml), was added to the cells. Polybrene (Cat# TR-1003, Sigma-Aldrich) was used to improve infection efficiency. HUVECs were incubated with lentiviruses for 24 hours. After transduction, the cells were resuspended in a fresh endothelial cell medium, cultured overnight, and used for further experiments. HUVECs expressing scrambled shRNA and HUVECs without virus treatment were used as controls for the PHGDH overexpression construct.

Protein extraction and Western blotting

HUVECs expressing either the PHGDH overexpression system or shControl gene were cultured in 6-well plates (5000 cells/cm^2) in endothelial cell medium supplemented with 1 µl/ml (vol/vol) ^{14}C-[1]-L-phenylalanine (see *Carbon-14 labeling* section). After 48 hours, cells were homogenized in lysis buffer containing 20 mM HEPES (pH 7.4), 1 mM EDTA, 5 mM EGTA, 10 mM $MgCl_2$, 100 mM β-glycerophosphate, 1 mM Na_3VO_4, 1 mM DTT, 1% TritonX-100, and supplemented with protease and phosphatase inhibitors (Cat# 78442, Thermo Fisher Scientific). Cell lysates were centrifuged for 5 min at 13,000 x g, 4 ℃, and the supernatant was collected. Separate aliquots of the supernatants were used for western blotting and analysis of ^{14}C-[1]-L-phenylalanine incorporation into proteins with liquid scintillation counting (see *Carbon-14 labeling* -section). Western blot analysis of PHGDH was conducted by using low-fluorescence PVDF membranes and anti-PHGDH antibody (1:5000 dilution, Cat# HPA021241, Sigma-Aldrich) as previously (27) with GAPDH (1:10 000 dilution, Cat# ab9485, Abcam) as a loading control.

Statistical testing in non-*omics* analyses

Statistical tests were conducted using GraphPad Prism 10.3.1 (Dotmatics). The Student's t-test was used when two groups were compared, whereas one-way ANOVA with Fisher's least significant difference test was used when a control group was compared to various treatment groups. The main effects and interaction of two variables were examined using two-way ANOVA. Group difference was considered statistically significant with $p \leq 0.05$.

Acknowledgments

We thank Associate Professor Thomas M. O'Connell for valuable advice regarding ^{13}C isotopic tracing and for providing the R script for ranking the significantly altered genes. We also thank all the laboratory technicians who helped us during this study. Figures 1A and 3A were created with the licensed version of https://www.biorender.com/.

CRediT authorship contribution statement

Sakari Mäntyselkä: Conceptualization, Methodology, Validation, Formal analysis, Investigation, Resources, Writing – Original Draft, Writing – Review & Editing, Visualization. **Erik Niemi**: Conceptualization, Methodology, Validation, Formal analysis,

Investigation, Data Curation, Writing – Original Draft, Writing – Review & Editing, Visualization. **Laura Ylä-Outinen:** Conceptualization, Methodology, Investigation, Writing – Review & Editing**. Kalle Kolari:** Investigation, Writing – Review & Editing. **Liina Uusitalo-Kylmälä:** Formal analysis, Investigation, Writing – Review & Editing, Visualization. **Alfredo Ortega-Alonso:** Formal Analysis, Data Curation, Writing – Review & Editing. **Roosa-Maria Liimatainen:** Validation, Investigation, Review of the manuscript. **Vasco Fachada:** Software, Writing – Review & Editing. **Perttu Permi:** Investigation, Writing – Review & Editing. **Elina Kalenius:** Methodology, Writing – Review & Editing, Supervision. **Juha J Hulmi:** Conceptualization, Resources, Writing – Original Draft, Writing – Review & Editing, Supervision, Project administration. **Riikka Kivelä:** Conceptualization, Resources, Writing – Original Draft, Writing – Review & Editing, Supervision, Project administration, Funding acquisition.

Funding

This work was supported by the Research Council of Finland (R.K., Grant number: 348636), the Sigrid Jusélius Foundation (R.K.), the Finnish Foundation for Cardiovascular Research (R.K., L. U-K.), the Emil Aaltonen Foundation (S.M., E.N.), and the Finnish Cultural Foundation (K.K. and J.J.H).

Disclosure and competing interest statement

The authors declare that they have no known competing financial interests or personal relationships that could have appeared to influence the work reported in this paper.

Supplementary Data

A PDF file containing Supplementary Figures 1-7.

Excel spreadsheets:

- Table S1: List of DEGs
- Table S2: Overlapping DEGs
- Table S3: GSEA results
- Table S4: Overlapping GSEA pathways
- Table S5: Metabolomics data
- Table S6: ^{13}C-(U)-glucose labeling data
- Table S7: MRM-transitions used in ^{13}C-(U)-glucose tracing

Data availability

Filtered non-aligned RNA sequencing data and non-normalized quantified reads are available in the Gene Expression Omnibus (GEO) data repository (accession number:

GSE288064). Processed transcriptomics data are shared as Supplementary Excel spreadsheets. Numerical metabolomics and isotopic tracing data are shared as Supplementary Excel spreadsheets.

References

1. Englund, D. A., Zhang, X., Aversa, Z., and LeBrasseur, N. K. (2021) Skeletal muscle aging, cellular senescence, and senotherapeutics: Current knowledge and future directions. *Mech. Ageing Dev.* **200**, 111595
2. Pepe, G. J. and Albrecht, E. D. (2023) Microvascular Skeletal-Muscle Crosstalk in Health and Disease. *Int. J. Mol. Sci.* **24**, 10425
3. Lautaoja, J. H., Turner, D. C., Sharples, A. P., Kivelä, R., Pekkala, S., Hulmi, J. J., and Ylä-Outinen, L. (2023) Mimicking exercise in vitro: effects of myotube contractions and mechanical stretch on omics. *Am. J. Physiol. Cell Physiol.* **324**, C886–C892
4. Yeo, R. X., Noone, J., and Sparks, L. M. (2024) Translating In Vitro Models of Exercise in Human Muscle Cells: A Mitocentric View. *Exerc. Sport Sci. Rev.* **52**, 3–12
5. Jufri, N. F., Mohamedali, A., Avolio, A., and Baker, M. S. (2015) Mechanical stretch: physiological and pathological implications for human vascular endothelial cells. *Vasc. Cell* **7**, 8
6. Ren, D., Song, J., Liu, R., Zeng, X., Yan, X., Zhang, Q., and Yuan, X. (2021) Molecular and Biomechanical Adaptations to Mechanical Stretch in Cultured Myotubes. *Front. Physiol.* **12**, 689492
7. Nakai, N., Kawano, F., and Nakata, K. (2015) Mechanical stretch activates mammalian target of rapamycin and AMP-activated protein kinase pathways in skeletal muscle cells. *Mol. Cell. Biochem.* **406**, 285–292
8. Turner, D. C., Gorski, P. P., Seaborne, R. A., Viggars, M., Murphy, M., Jarvis, J. C., Martin, N. R. W., Stewart, C. E., and Sharples, A. P. (2021) Mechanical loading of bioengineered skeletal muscle in vitro recapitulates gene expression signatures of resistance exercise in vivo. *J. Cell. Physiol.* **236**, 6534–6547
9. Große-Segerath, L., Follert, P., Behnke, K., Ettich, J., Buschmann, T., Kirschner, P., Hartwig, S., Lehr, S., Korf-Klingebiel, M., Eberhard, D., Lehwald-Tywuschik, N., Al-Hasani, H., Knoefel, W. T., Heinrich, S., Levkau, B., Wollert, K. C., Scheller, J., and Lammert, E. (2024) Identification of myeloid-derived growth factor as a mechanically-induced, growth-promoting angiocrine signal for human hepatocytes. *Nat. Commun.* **15**, 1076
10. Lorenz, L., Axnick, J., Buschmann, T., Henning, C., Urner, S., Fang, S., Nurmi, H., Eichhorst, N., Holtmeier, R., Bódis, K., Hwang, J.-H., Müssig, K., Eberhard, D., Stypmann, J., Kuss, O., Roden, M., Alitalo, K., Häussinger, D., and Lammert, E. (2018) Mechanosensing by β1 integrin induces angiocrine signals for liver growth and survival. *Nature* **562**, 128–132
11. Biernat, K., Kuciel, N., Mazurek, J., and Hap, K. (2024) Is It Possible to Train the Endothelium?-A Narrative Literature Review. *Life Basel Switz.* **14**, 616
12. Sottiurai, V. S., Sue, S. L., Breaux, J. R., and Smith, L. M. (1989) Adaptability of endothelial orientation to blood flow dynamics--a morphologic analysis. *Eur. J. Vasc. Surg.* **3**, 145–151
13. Hinkle, E. R., Blue, R. E., Tsai, Y.-H., Combs, M., Davi, J., Coffey, A. R., Boriek, A. M., Taylor, J. M., Parker, J. S., and Giudice, J. (2022) Stretching muscle cells induces

transcriptional and splicing transitions and changes in SR proteins. *Commun. Biol.* **5**, 987

14. Ilaiwy, A., Quintana, M. T., Bain, J. R., Muehlbauer, M. J., Brown, D. I., Stansfield, W. E., and Willis, M. S. (2016) Cessation of biomechanical stretch model of C2C12 cells models myocyte atrophy and anaplerotic changes in metabolism using non-targeted metabolomics analysis. *Int. J. Biochem. Cell Biol.* **79**, 80–92
15. Smith, J. A. B., Murach, K. A., Dyar, K. A., and Zierath, J. R. (2023) Exercise metabolism and adaptation in skeletal muscle. *Nat. Rev. Mol. Cell Biol.* **24**, 607–632
16. Li, S., Xu, Z., Wang, Y., Chen, L., Wang, X., Zhou, Y., Lei, D., Zang, G., and Wang, G. (2024) Recent advances of mechanosensitive genes in vascular endothelial cells for the formation and treatment of atherosclerosis. *Genes Dis.* **11**, 101046
17. Davis, M. J., Earley, S., Li, Y.-S., and Chien, S. (2023) Vascular mechanotransduction. *Physiol. Rev.* **103**, 1247–1421
18. Peng, Z., Shu, B., Zhang, Y., and Wang, M. (2019) Endothelial Response to Pathophysiological Stress. *Arterioscler. Thromb. Vasc. Biol.* **39**, e233–e243
19. Pillon, N. J., Gabriel, B. M., Dollet, L., Smith, J. A. B., Sardón Puig, L., Botella, J., Bishop, D. J., Krook, A., and Zierath, J. R. (2020) Transcriptomic profiling of skeletal muscle adaptations to exercise and inactivity. *Nat. Commun.* **11**, 470
20. Smith, J. A. B., Gabriel, B. M., Brady, A. J., Abdelmoez, A. M., Savikj, M., Wright, S. C., Koutsilieri, S., Barrès, R., Lauschke, V. M., Krook, A., Zierath, J. R., and Pillon, N. J. (2025) Inactivity-induced NR4A3 downregulation in human skeletal muscle affects glucose metabolism and translation: Insights from in vitro analysis. *Mol. Metab.* **99**, 102200
21. Hulmi, J. J., Ahtiainen, J. P., Kaasalainen, T., Pöllänen, E., Häkkinen, K., Alen, M., Selänne, H., Kovanen, V., and Mero, A. A. (2007) Postexercise myostatin and activin IIb mRNA levels: effects of strength training. *Med. Sci. Sports Exerc.* **39**, 289–297
22. Kim, J., Cross, J. M., and Bamman, M. M. (2005) Impact of resistance loading on myostatin expression and cell cycle regulation in young and older men and women. *Am. J. Physiol. Endocrinol. Metab.* **288**, E1110-1119
23. Hood, D. A., Tryon, L. D., Carter, H. N., Kim, Y., and Chen, C. C. W. (2016) Unravelling the mechanisms regulating muscle mitochondrial biogenesis. *Biochem. J.* **473**, 2295–2314
24. Fan, W. and Evans, R. (2015) PPARs and ERRs: molecular mediators of mitochondrial metabolism. *Curr. Opin. Cell Biol.* **33**, 49–54
25. Wickramasinghe, N. M., Sachs, D., Shewale, B., Gonzalez, D. M., Dhanan-Krishnan, P., Torre, D., LaMarca, E., Raimo, S., Dariolli, R., Serasinghe, M. N., Mayourian, J., Sebra, R., Beaumont, K., Iyengar, S., French, D. L., Hansen, A., Eschenhagen, T., Chipuk, J. E., Sobie, E. A., Jacobs, A., Akbarian, S., Ischiropoulos, H., Ma'ayan, A., Houten, S. M., Costa, K., and Dubois, N. C. (2022) PPARdelta activation induces metabolic and contractile maturation of human pluripotent stem cell-derived cardiomyocytes. *Cell Stem Cell* **29**, 559-576.e7
26. Vandekeere, S., Dubois, C., Kalucka, J., Sullivan, M. R., García-Caballero, M., Goveia, J., Chen, R., Diehl, F. F., Bar-Lev, L., Souffreau, J., Pircher, A., Kumar, S., Vinckier, S., Hirabayashi, Y., Furuya, S., Schoonjans, L., Eelen, G., Ghesquière, B., Keshet, E., Li, X., Vander Heiden, M. G., Dewerchin, M., and Carmeliet, P. (2018) Serine Synthesis via PHGDH Is Essential for Heme Production in Endothelial Cells. *Cell Metab.* **28**, 573-587.e13

27. Mäntyselkä, S., Kolari, K., Baumert, P., Ylä-Outinen, L., Kuikka, L., Lahtonen, S., Permi, P., Wackerhage, H., Kalenius, E., Kivelä, R., and Hulmi, J. J. (2024) Serine synthesis pathway enzyme PHGDH is critical for muscle cell biomass, anabolic metabolism, and mTORC1 signaling. *Am. J. Physiol. Endocrinol. Metab.* **326**, E73–E91
28. Mäntyselkä, S., Ahvenlammi, M., Vartiainen, J., Halonen, E. J., Kolari, K., Wackerhage, H., Permi, P., Varjosalo, M., Kelahaara, M. M., Ahtiainen, J. P., Kalenius, E., Kivelä, R., and Hulmi, J. J. (2025) Glycolytic metabolism and biomass production from glucose in human skeletal muscle growth. *Am. J. Physiol. Cell Physiol.*
29. Lautaoja, J. H., M O'Connell, T., Mäntyselkä, S., Peräkylä, J., Kainulainen, H., Pekkala, S., Permi, P., and Hulmi, J. J. (2021) Higher glucose availability augments the metabolic responses of the C2C12 myotubes to exercise-like electrical pulse stimulation. *Am. J. Physiol. Endocrinol. Metab.* **321**, E229–E245
30. van Hall, G., Sacchetti, M., and Rådegran, G. (2002) Whole body and leg acetate kinetics at rest, during exercise and recovery in humans. *J. Physiol.* **542**, 263–272
31. Schranner, D., Kastenmüller, G., Schönfelder, M., Römisch-Margl, W., and Wackerhage, H. (2020) Metabolite Concentration Changes in Humans After a Bout of Exercise: a Systematic Review of Exercise Metabolomics Studies. *Sports Med. - Open* **6**, 11
32. Kujala, U. M., Mäkinen, V.-P., Heinonen, I., Soininen, P., Kangas, A. J., Leskinen, T. H., Rahkila, P., Würtz, P., Kovanen, V., Cheng, S., Sipilä, S., Hirvensalo, M., Telama, R., Tammelin, T., Savolainen, M. J., Pouta, A., O'Reilly, P. F., Mäntyselkä, P., Viikari, J., Kähönen, M., Lehtimäki, T., Elliott, P., Vanhala, M. J., Raitakari, O. T., Järvelin, M.-R., Kaprio, J., Kainulainen, H., and Ala-Korpela, M. (2013) Long-term leisure-time physical activity and serum metabolome. *Circulation* **127**, 340–348
33. Jing, X., Lyu, J., and Xiong, J. (2023) Acetate regulates GAPDH acetylation and T helper 1 cell differentiation. *Mol. Biol. Cell* **34**, br10
34. Miller, K. D., O'Connor, S., Pniewski, K. A., Kannan, T., Acosta, R., Mirji, G., Papp, S., Hulse, M., Mukha, D., Hlavaty, S. I., Salcido, K. N., Bertolazzi, F., Srikanth, Y. V. V., Zhao, S., Wellen, K. E., Shinde, R. S., Claiborne, D. T., Kossenkov, A., Salvino, J. M., and Schug, Z. T. (2023) Acetate acts as a metabolic immunomodulator by bolstering T-cell effector function and potentiating antitumor immunity in breast cancer. *Nat. Cancer* **4**, 1491–1507
35. Qiu, J., Villa, M., Sanin, D. E., Buck, M. D., O'Sullivan, D., Ching, R., Matsushita, M., Grzes, K. M., Winkler, F., Chang, C.-H., Curtis, J. D., Kyle, R. L., Van Teijlingen Bakker, N., Corrado, M., Haessler, F., Alfei, F., Edwards-Hicks, J., Maggi, L. B., Zehn, D., Egawa, T., Bengsch, B., Klein Geltink, R. I., Jenuwein, T., Pearce, E. J., and Pearce, E. L. (2019) Acetate Promotes T Cell Effector Function during Glucose Restriction. *Cell Rep.* **27**, 2063-2074.e5
36. Chastin, S. F. M., Abaraogu, U., Bourgois, J. G., Dall, P. M., Darnborough, J., Duncan, E., Dumortier, J., Pavón, D. J., McParland, J., Roberts, N. J., and Hamer, M. (2021) Effects of Regular Physical Activity on the Immune System, Vaccination and Risk of Community-Acquired Infectious Disease in the General Population: Systematic Review and Meta-Analysis. *Sports Med. Auckl. NZ* **51**, 1673–1686
37. Kwee, B. J., Budina, E., Najibi, A. J., and Mooney, D. J. (2018) CD4 T-cells regulate angiogenesis and myogenesis. *Biomaterials* **178**, 109–121

38. Schiaffino, S., Pereira, M. G., Ciciliot, S., and Rovere-Querini, P. (2017) Regulatory T cells and skeletal muscle regeneration. *FEBS J.* **284**, 517–524
39. Horibata, Y., Ando, H., Itoh, M., and Sugimoto, H. (2013) Enzymatic and transcriptional regulation of the cytoplasmic acetyl-CoA hydrolase ACOT12. *J. Lipid Res.* **54**, 2049–2059
40. Liu, X., Cooper, D. E., Cluntun, A. A., Warmoes, M. O., Zhao, S., Reid, M. A., Liu, J., Lund, P. J., Lopes, M., Garcia, B. A., Wellen, K. E., Kirsch, D. G., and Locasale, J. W. (2018) Acetate Production from Glucose and Coupling to Mitochondrial Metabolism in Mammals. *Cell* **175**, 502-513.e13
41. Bose, S., Ramesh, V., and Locasale, J. W. (2019) Acetate Metabolism in Physiology, Cancer, and Beyond. *Trends Cell Biol.* **29**, 695–703
42. Powers, S. K., Radak, Z., Ji, L. L., and Jackson, M. (2024) Reactive oxygen species promote endurance exercise-induced adaptations in skeletal muscles. *J. Sport Health Sci.* **13**, 780–792
43. De Bock, K., Georgiadou, M., Schoors, S., Kuchnio, A., Wong, B. W., Cantelmo, A. R., Quaegebeur, A., Ghesquière, B., Cauwenberghs, S., Eelen, G., Phng, L.-K., Betz, I., Tembuyser, B., Brepoels, K., Welti, J., Geudens, I., Segura, I., Cruys, B., Bifari, F., Decimo, I., Blanco, R., Wyns, S., Vangindertael, J., Rocha, S., Collins, R. T., Munck, S., Daelemans, D., Imamura, H., Devlieger, R., Rider, M., Van Veldhoven, P. P., Schuit, F., Bartrons, R., Hofkens, J., Fraisl, P., Telang, S., Deberardinis, R. J., Schoonjans, L., Vinckier, S., Chesney, J., Gerhardt, H., Dewerchin, M., and Carmeliet, P. (2013) Role of PFKFB3-driven glycolysis in vessel sprouting. *Cell* **154**, 651–663
44. Hammarström, D., Øfsteng, S. J., Jacobsen, N. B., Flobergseter, K. B., Rønnestad, B. R., and Ellefsen, S. (2022) Ribosome accumulation during early phase resistance training in humans. *Acta Physiol.* **235**, e13806
45. Verma, M., Asakura, Y., Murakonda, B. S. R., Pengo, T., Latroche, C., Chazaud, B., McLoon, L. K., and Asakura, A. (2018) Muscle Satellite Cell Cross-Talk with a Vascular Niche maintains quiescence via VEGF and Notch Signaling. *Cell Stem Cell* **23**, 530-543.e9
46. Addington, A. K., Wall, R. M., Wei, X., Frate, S. D., Olsen, M. L., Drake, J. C., and Craige, S. M. (2025) Distinct endothelial gene responses to acute exercise in skeletal muscle. *Am. J. Physiol.-Endocrinol. Metab.* **329**, E560–E570
47. Wang, J.-Y., Lee, Y.-T., Chang, P.-F., and Chau, L.-Y. (2009) Hemin promotes proliferation and differentiation of endothelial progenitor cells via activation of AKT and ERK. *J. Cell. Physiol.* **219**, 617–625
48. Halonen, E. J., Gabriel, I., Kelahaara, M. M., Ahtiainen, J. P., and Hulmi, J. J. (2024) Does Taking a Break Matter-Adaptations in Muscle Strength and Size Between Continuous and Periodic Resistance Training. *Scand. J. Med. Sci. Sports* **34**, e14739
49. Legrand, C., Bour, J. M., Jacob, C., Capiaumont, J., Martial, A., Marc, A., Wudtke, M., Kretzmer, G., Demangel, C., and Duval, D. (1992) Lactate dehydrogenase (LDH) activity of the cultured eukaryotic cells as marker of the number of dead cells in the medium [corrected]. *J. Biotechnol.* **25**, 231–243
50. Langmead, B. and Salzberg, S. L. (2012) Fast gapped-read alignment with Bowtie 2. *Nat. Methods* **9**, 357–359

51. Liao, Y., Smyth, G. K., and Shi, W. (2014) featureCounts: an efficient general purpose program for assigning sequence reads to genomic features. *Bioinforma. Oxf. Engl.* **30**, 923–930
52. Robinson, M. D., McCarthy, D. J., and Smyth, G. K. (2010) edgeR: a Bioconductor package for differential expression analysis of digital gene expression data. *Bioinforma. Oxf. Engl.* **26**, 139–140
53. Chen, Y., Lun, A. T. L., and Smyth, G. K. (2016) From reads to genes to pathways: differential expression analysis of RNA-Seq experiments using Rsubread and the edgeR quasi-likelihood pipeline. *F1000Research* **5**, 1438
54. Robinson, M. D. and Oshlack, A. (2010) A scaling normalization method for differential expression analysis of RNA-seq data. *Genome Biol.* **11**, R25
55. Ritchie, M. E., Phipson, B., Wu, D., Hu, Y., Law, C. W., Shi, W., and Smyth, G. K. (2015) limma powers differential expression analyses for RNA-sequencing and microarray studies. *Nucleic Acids Res.* **43**, e47
56. Law, C. W., Chen, Y., Shi, W., and Smyth, G. K. (2014) voom: Precision weights unlock linear model analysis tools for RNA-seq read counts. *Genome Biol.* **15**, R29
57. Yu, G., Wang, L.-G., Han, Y., and He, Q.-Y. (2012) clusterProfiler: an R package for comparing biological themes among gene clusters. *Omics J. Integr. Biol.* **16**, 284–287
58. Ge, S. X., Jung, D., and Yao, R. (2020) ShinyGO: a graphical gene-set enrichment tool for animals and plants. *Bioinforma. Oxf. Engl.* **36**, 2628–2629
59. Qasem, R. J., Farh, I. K., and Al Essa, M. A. (2017) A novel LC-MS/MS method for the quantitative measurement of the acetate content in pharmaceutical peptides. *J. Pharm. Biomed. Anal.* **146**, 354–360
60. Tsugawa, H., Kanazawa, M., Ogiwara, A., and Arita, M. (2014) MRMPROBS suite for metabolomics using large-scale MRM assays. *Bioinforma. Oxf. Engl.* **30**, 2379–2380
61. Millard, P., Delépine, B., Guionnet, M., Heuillet, M., Bellvert, F., and Létisse, F. (2019) IsoCor: isotope correction for high-resolution MS labeling experiments. *Bioinforma. Oxf. Engl.* **35**, 4484–4487
62. Yoon, S. J., Combs, J. A., Falzone, A., Prieto-Farigua, N., Caldwell, S., Ackerman, H. D., Flores, E. R., and DeNicola, G. M. (2023) Comprehensive Metabolic Tracing Reveals the Origin and Catabolism of Cysteine in Mammalian Tissues and Tumors. *Cancer Res.* **83**, 1426–1442
63. Zhang, T., Gillies, M. C., Madigan, M. C., Shen, W., Du, J., Grünert, U., Zhou, F., Yam, M., and Zhu, L. (2018) Disruption of De Novo Serine Synthesis in Müller Cells Induced Mitochondrial Dysfunction and Aggravated Oxidative Damage. *Mol. Neurobiol.* **55**, 7025–7037
64. Białopiotrowicz, E., Noyszewska-Kania, M., Kachamakova-Trojanowska, N., Łoboda, A., Cybulska, M., Grochowska, A., Kopczyński, M., Mikula, M., Prochorec-Sobieszek, M., Firczuk, M., Graczyk-Jarzynka, A., Zagożdżon, R., Ząbek, A., Młynarz, P., Dulak, J., Górniak, P., Szydłowski, M., Pyziak, K., Martyka, J., Sroka-Porada, A., Jabłońska, E., Polak, A., Kowalczyk, P., Szumera-Ciećkiewicz, A., Chapuy, B., Rzymski, T., Brzózka, K., and Juszczyński, P. (2020) Serine Biosynthesis Pathway Supports MYC-miR-494-EZH2 Feed-Forward Circuit Necessary to Maintain Metabolic and Epigenetic Reprogramming of Burkitt Lymphoma Cells. *Cancers* **12**, 580

1030 65. Zhang, X., Sun, M., Jiao, Y., Lin, B., and Yang, Q. (2022) PHGDH Inhibitor CBR-5884
1031 Inhibits Epithelial Ovarian Cancer Progression via ROS/Wnt/β-Catenin Pathway and
1032 Plays a Synergistic Role with PARP Inhibitor Olaparib. *Oxid. Med. Cell. Longev.* **2022**,
1033 9029544
1034 66. Pacold, M. E., Brimacombe, K. R., Chan, S. H., Rohde, J. M., Lewis, C. A., Swier, L. J.
1035 Y. M., Possemato, R., Chen, W. W., Sullivan, L. B., Fiske, B. P., Cho, S., Freinkman,
1036 E., Birsoy, K., Abu-Remaileh, M., Shaul, Y. D., Liu, C. M., Zhou, M., Koh, M. J., Chung,
1037 H., Davidson, S. M., Luengo, A., Wang, A. Q., Xu, X., Yasgar, A., Liu, L., Rai, G.,
1038 Westover, K. D., Vander Heiden, M. G., Shen, M., Gray, N. S., Boxer, M. B., and
1039 Sabatini, D. M. (2016) A PHGDH inhibitor reveals coordination of serine synthesis
1040 and one-carbon unit fate. *Nat. Chem. Biol.* **12**, 452–458
1041